

Hamiltonian Control Design for DC Microgrids with Stochastic Sources and Loads with Applications

David G. Wilson, Jason C. Neely, Marvin A. Cook, Steven F. Glover

*Electrical Science and Experiments Department, Sandia National Laboratories,
P.O. Box 5800, Albuquerque, NM 87185-1152, [dwilso, jneely, macook, sfglove]@sandia.gov*

Joseph Young

OptimoJoe, P.O. Box 19053, Albuquerque, NM 87119, joe@optimojoe.com

Rush D. Robinett III

*R.L. Smith Bldg 903, 1400 Townsend Drive,
Michigan Technological University, Houghton, MI 49931, rdrobine@mtu.edu*

Abstract—To achieve high performance operation of microgrids that contain stochastic sources and loads is a challenge that will impact cost and complexity. Developing alternative methods for controlling and analyzing these systems will provide insight into tradeoffs that can be made during the design phase. This paper presents a design methodology, based on Hamiltonian Surface Shaping and Power Flow Control (HSSPFC) [1] for a hierarchical control scheme that regulates renewable energy sources and energy storage in a DC microgrid. Recent literature has indicated that there exists a trade-off in information and power flow and that intelligent, coordinated control of power flow in a microgrid system can modify energy storage hardware requirements. Two scenarios are considered; i) simple two stochastic source with variable load renewable DC Microgrid example and ii) a three zone electric ship with DC Microgrid and varying pulse load profiles.

Keywords - decentralized control; microgrid; nonlinear control; energy storage; stochastic sources

I. INTRODUCTION

The electric power grid is evolving to a state which has yet to be defined. Unidirectional power and information flow will be replaced by bi-directional flow as new generation sources distribute throughout the electric grid of the future. Renewable and other distributed energy sources cannot be economically and reliably integrated into the existing grid because it has been optimized over decades to large centralized generation sources. Today's grid model is based on excess generation capacity (largely fossil fuel), static distribution/transmission systems, and essentially open loop control of power flow between sources and loads. Research investments in grid modernization and microgrids are presently being made by the Department of Energy, Department of Defense, industry, universities, and others [1], [2], [3], [4], [5], [6]. Emphasis of this research is to develop mathematical tools that can optimize designs specific to an application.

Achieving regulation and power balance in a system with high penetration levels of stochastic renewable sources are some of the challenges addressed by this research. The problem is solved provided enough energy storage is available; unfortunately, energy storage systems incur cost,

and the minimum required energy storage is dependent on performance objectives. Herein, the problem of increasing renewable energy penetration in a microgrid is addressed. The proposed method distributes the control of energy storage and power converters and attempts to minimize energy storage using controls. In effect, the physical energy storage may be mitigated by increasing information flow between controllers [1].

Regulation of energy storage and power conversion in the microgrid is divided into three parts: the guidance control, the Hamiltonian-based control, and the servo control. A centralized controller provides guidance control by computing reference duty cycle values and reference states that optimize some criteria (ie. minimizes some cost function or maximizes some value function); the guidance control identifies the optimal operating point and is determined using Sequential Quadratic Programming (SQP) or dynamic programming methods [7], [8]. The Hamiltonian-based control is a local feedback controller that is designed to minimize variability in the power delivered to the boost converters [1], [7], [9], [10]. The servo control supports the Hamiltonian-based control by regulating certain components to specified voltages. In this paper the Secure Scalable Microgrid (SSM) hardware testbed and descriptions are presented in Section II. A dynamic optimization planner for guidance control is introduced in Section III. A HSSPFC control design is given in Section IV. Experimental results are discussed in Section V and Section VI reviews multiple microgrid system configurations and finally, Section VII provides conclusions.

II. MICROGRID SYSTEM AND REDUCED ORDER MODEL

A comprehensive microgrid testbed has been constructed which includes a reconfigurable bus, two mechanical source emulators capable of emulating a wind turbine, diesel engine, water turbine, or a wave energy device, a high-power digital resistor rated to 6.7 kW at 400V bus voltage, an energy storage emulator capable of sourcing or sinking 5kW of power, and master control console that scripts the experiments [11], [12], [13], [14]. The system under consideration for this paper has two wind turbine generators, three energy

storage systems and a resistive load; see Figs. 1 and 21 (see Appendix). Figure 2 shows a screenshot from the master control console control software depicting a simple experiment that includes multiple emulator profiles (i.e., wind speed) and a load profile. As will be explained in the next section, the control scheme has three layers including a guidance control, a Hamiltonian-based control and a servo control. The servo-control operates on the fastest timescale.

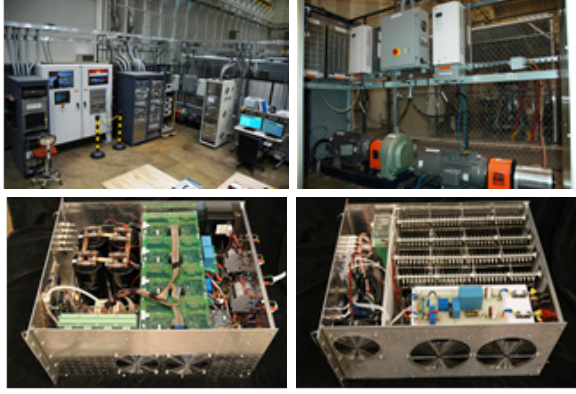


Fig. 1. Photos: microgrid testbed (upper left) mechanical source emulators (upper right), energy storage emulator (lower left), and high power digital resistor (lower right), respectively.

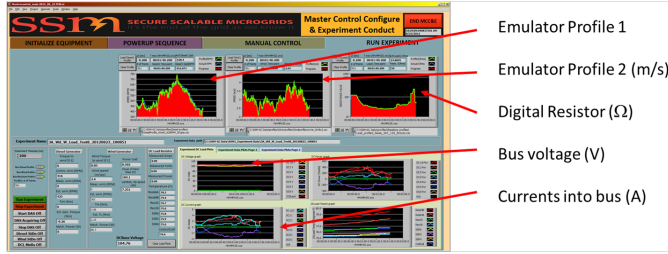


Fig. 2. Demonstration of simple experiment from master control console with HSSPFC control.

Since voltages u_1 and u_2 are maintained using the servo-controller, the simplified model [7] for Hamiltonian control is:

$$\begin{bmatrix} L_1 & 0 & 0 \\ 0 & L_2 & 0 \\ 0 & 0 & C_t \end{bmatrix} \begin{Bmatrix} \dot{i}_{L_1} \\ \dot{i}_{L_2} \\ \dot{v}_{bus} \end{Bmatrix} = \begin{bmatrix} -r_{L_1} & 0 & -\lambda_1 \\ 0 & -r_{L_2} & -\lambda_2 \\ \lambda_1 & \lambda_2 & -G_L \end{bmatrix} \begin{Bmatrix} i_{L_1} \\ i_{L_2} \\ v_{bus} \end{Bmatrix} + \begin{Bmatrix} v_1 \\ v_2 \\ 0 \end{Bmatrix} + \begin{Bmatrix} u_1 \\ u_2 \\ u_3 \end{Bmatrix} \quad (1)$$

where λ_1 and λ_2 are right side duty-cycles for the first and second boost converters, respectively. R_{load} is assumed piecewise constant and all L, C , and remaining resistor values are assumed constant and Eq. (1) can be written in matrix form as

$$\mathbf{M}\dot{\mathbf{x}} = [\bar{\mathbf{A}}(R_{load}) + \tilde{\mathbf{A}}(\lambda)] \mathbf{x} + \mathbf{v} + \mathbf{u}$$

or

$$\mathbf{M}\dot{\mathbf{x}} = \mathbf{R}\mathbf{x} + \mathbf{v} + \mathbf{u} \quad (2)$$

where $\lambda = [\lambda_1 \ \lambda_2]^T$, $\bar{\mathbf{A}}(R_{load})$ is a diagonal matrix, and $\tilde{\mathbf{A}}(\lambda)$ is a skew-symmetric matrix.

III. DYNAMIC OPTIMIZER/PLANNER

For the guidance algorithm either the steady-state solution to Eq. (2) can be solved [7] or for this discussion a dynamic optimization formulation is reviewed. Utilizing the model [7] for a single DC microgrid or Eq. (2) the optimal control problem is developed with the following performance index (PI)

$$PI = \frac{w_1}{2} \|\lambda - \lambda_0\|^2 + \frac{w_2}{2} \|\mathbf{w}_u \circ \mathbf{u}\|^2 + \frac{w_3}{2} \mathbf{i}^T \text{Diag}(\mathbf{R}) \mathbf{i} + \frac{w_4}{2} (\mathbf{x}^T (\mathbf{w}_u \circ \mathbf{u}))^2 \quad (3)$$

which includes multiple objectives to minimize for $\dot{\lambda}, \lambda, \dot{\mathbf{x}}, \mathbf{x}, \mathbf{u}, v_B, \mathbf{i}$ subject to the circuit equations $\mathbf{M}\dot{\mathbf{x}} = [\bar{\mathbf{A}} + \tilde{\mathbf{A}}(\lambda)]\mathbf{x} + \mathbf{v} + (\mathbf{w}_u \circ \mathbf{u})$, with $\mathbf{x} = [\mathbf{i} \ v_B]^T$ and the discretization equations given as $\mathbf{x} = \mathbf{x}_0 + \Delta t \dot{\mathbf{x}}$ and $\lambda = \lambda_0 + \Delta t \dot{\lambda}$. The parameter bounds become

$$\begin{aligned} \mathbf{i}_{\min} &\leq \mathbf{i} \leq \mathbf{i}_{\max} \\ \mathbf{u}_{\min} &\leq \mathbf{w}_u \circ \mathbf{u} \leq \mathbf{u}_{\max} \\ \lambda_{\min} &\leq \lambda \leq \lambda_{\max} \end{aligned}$$

where \circ denotes the pointwise product. In this formulation, one can minimize either the change in the boost converter duty cycle (w_1), the amount of storage used by the microgrid (w_2), the parasitic losses (w_3), or the amount of power (w_4). The weights, $w_i, i = 1 \dots 4$, are selected to determine which combination of objectives to optimize. The formulation is constrained by the circuit equations for the microgrid, the definition of the auxiliary variable \mathbf{x} , a discretization in time, and by bounds on the individual parameters. As a final note, in order to remove a storage device from a boost converter, a weighting \mathbf{w}_u is introduced. When one sets the corresponding element to 0 that particular storage element is eliminated.

In order to solve the optimization formulation, we use an optimization solver called Optizelle[15] and apply an inexact composite step SQP trust-region algorithm combined with a primal-dual interior-point method. This allows us to solve the optimal control problem in roughly 20 – 30 iterations.

As an example, consider the two boost converter microgrid where the storage on the first boost converter is eliminated. To minimize the change in the boost converter duty cycles, Optizelle took 29 iterations to converge, as shown in Fig. 3.

Iter	f(x)	grad	dx	g(x)	mu_est
1	0.00e+00	1.29e-13	---	9.20e+01	1.00e+00
2	3.25e-02	3.12e-04	2.60e+02	5.29e+01	5.61e-01
3	7.30e-02	4.33e-05	8.50e+01	2.51e+01	3.33e-01
...					
27	1.90e-14	3.73e-09	3.05e+00	6.53e-07	7.66e-08
28	4.90e-13	3.64e-12	2.72e+01	5.37e-07	7.65e-08
29	4.91e-13	4.29e-17	9.11e-01	5.36e-07	7.65e-08

Fig. 3. Optizelle numerical convergence single microgrid results

IV. HAMILTONIAN SURFACE SHAPING AND POWER FLOW CONTROL

The system error state and control inputs are defined as $\tilde{\mathbf{x}} = \mathbf{x}_{\text{ref}} - \mathbf{x}$ and $\tilde{\mathbf{u}} = \mathbf{u}_{\text{ref}} - \mathbf{u}$. Given a load resistance R_{load} and variable stochastic sources \mathbf{v} , the reference values are computed first by setting $\mathbf{x} = \mathbf{0}$, $v_{\text{bus}} = (v_{\text{bus}})_{\text{ref}}$, and $\mathbf{u} = \mathbf{0}$ then solving the following for λ and \mathbf{x}_{ref} as [7]:

$$\left[\bar{\mathbf{A}}(R_{\text{load}}) + \tilde{\mathbf{A}}(\lambda) \right] \mathbf{x}_{\text{ref}} + \mathbf{v} = \mathbf{0}. \quad (4)$$

The feedback control is developed using a Hamiltonian formulation [7]. The reference input takes the form given as

$$\mathbf{u}_{\text{ref}} = - \left[\bar{\mathbf{A}}(R_{\text{load}}) + \tilde{\mathbf{A}}(\lambda) \right] \mathbf{x}_{\text{ref}} - \mathbf{v} \quad (5)$$

and the Hamiltonian is defined as

$$\mathcal{H} = \frac{1}{2} \tilde{\mathbf{x}}^T \mathbf{M} \tilde{\mathbf{x}} + \frac{1}{2} \left(\int_0^t \tilde{\mathbf{x}} d\tau \right)^T \mathbf{K}_I \left(\int_0^t \tilde{\mathbf{x}} d\tau \right) \quad (6)$$

where \mathbf{K}_I is a positive definite controller gain. Since \mathbf{M} is positive definite, the static stability condition is met [7]. For dynamic stability, the condition $\dot{\mathcal{H}} < 0$ must be met and is done through proper definition of the feedback control law which may take the form of a Proportional-Integral (PI) control [7]:

$$\tilde{\mathbf{u}} = -\mathbf{K}_P \tilde{\mathbf{x}} - \mathbf{K}_I \int_0^t \tilde{\mathbf{x}} d\tau. \quad (7)$$

The resulting time derivative of the Hamiltonian is given by:

$$\dot{\mathcal{H}} = \tilde{\mathbf{x}}^T \left[\mathbf{M} \dot{\tilde{\mathbf{x}}} + \mathbf{K}_I \left(\int_0^t \tilde{\mathbf{x}} d\tau \right) \right] = \tilde{\mathbf{x}}^T \left[\bar{\mathbf{A}}(R_{\text{load}}) - \mathbf{K}_P \right] \tilde{\mathbf{x}}. \quad (8)$$

Solution to Eqs. (4) and (5) (which includes the determination of λ) constitutes the guidance command and the solution is fully coupled in the states [7]. The control law for $\tilde{\mathbf{u}}$ in Eq. (7) that satisfies $\dot{\mathcal{H}} < 0$ constitutes the Hamiltonian-based control and is dynamically stable decoupled distributed control or

$$\bar{\mathbf{A}}(R_{\text{load}}) - \mathbf{K}_P < 0 \quad (9)$$

is used as a guide to select the controller gains \mathbf{K}_P .

The $\tilde{\mathbf{u}}$ commands are realized by a servo-controller that manages the energy storage units with a closed-loop bandwidth sufficiently high to satisfy the separation principle.

V. SINGLE DC MICROGRID EXPERIMENTAL RESULTS

In this section two primary scenarios are reviewed. The first scenario reviews communication update rates with and without energy storage. The second scenario reviews two stochastic wind inputs and with a stochastic load. Energy storage is included as part of one of the wind sources (u_1) and one directly on the DC bus (u_3 , note, for this experiment $u_2 = 0$).

A. Effects of communication rate without energy storage

Without an energy storage system to regulate bus voltage, the system relies heavily on timely updates from the informatic control layer. Specifically, the informatic control layer consolidates output current information from all sources and applies a filter to estimate load resistance. The informatic control then updates λ duty cycle values and reference inductor currents $i_{L_a}^*$. If the load and renewable sources contain abrupt changes, latencies can result in considerable bus voltage disturbances.

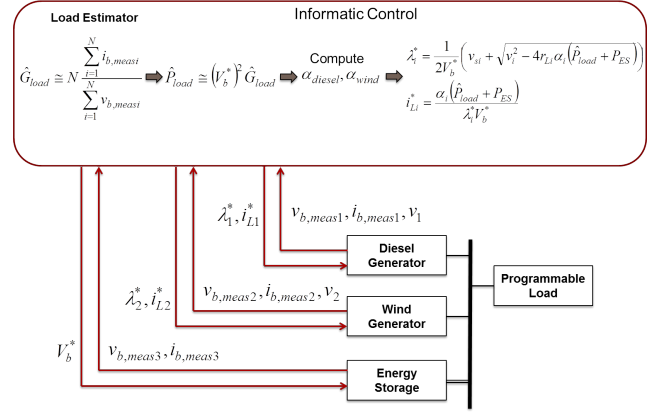


Fig. 4. Overview of informatic control for experiments (note the energy storage block is not activated for without energy storage option).

In this first set of four experiments, a single microgrid with diesel generation, wind generation and variable load was considered. A 100 V reference bus voltage and 100 second run time were selected, the diesel engine emulator was set for a constant 600 RPM and the same load profile and wind profile were utilized in each, but the update rate of the Informatic control was varied with update rates of: 1 Hz, 2 Hz, 10 Hz 100 Hz. Figure 4 shows an overview of the informatic controller operation. Figs. 5 and 6 shows the wind speed and load profiles used in this experiment; for clarity, the load admittance is shown instead of the load resistance ($G_{load} = 1/R_{load}$) since there is a clearer relationship between load admittance and load current. The time step for the profiles is 200 msec. Figures 7 and 8 show the resulting voltage and load current response for each update rate used by the informatic control. As expected, less frequent updates to the control policy result in considerable bus voltage disturbances, particularly for 1 Hz and 2 Hz.

In order to quantify the effect of update rates on the bus voltage disturbances, a cost function was defined as follows

$$J = \int_{t_0}^{t_f} (v_{bus}(\tau) - E(v_{bus}))^2 d\tau \quad (10)$$

which computes the squared error between the bus voltage and its average value $E(v_{bus})$ over the 100 second length of the experiment. The computed costs are plotted in Fig. 9 as a function of update rate. For comparison, the results are computed with other key frequency response values, including the servo controller closed loop control bandwidth,

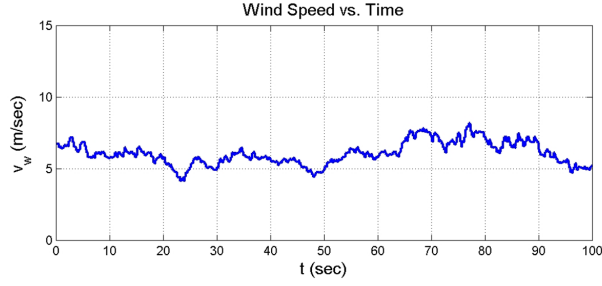


Fig. 5. Wind speed profile used in experiment.

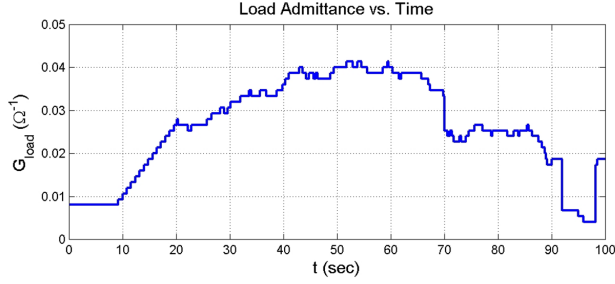


Fig. 6. Load admittance profile used in experiment.

the Nyquist frequency of the variable resistor updates (the profile had a 200 msec update rate), and the RC cutoff frequencies of the microgrid bus given the min and max load resistance values.

B. Effects of communication rate with energy storage

Similar to the previous experiment, the effect of update rate was further investigated for a system with a bus-tied energy-storage system, an ARESE-A, (Arbitrary Response Energy Storage Emulator, with A and B configurations that denote current or voltage sources, respectively) regulating bus voltage. In this implementation, the bus voltage is well regulated, but the control update rate impacts the control effort of the energy storage system; the controller configuration is illustrated in Fig. 4. Seven different update rates were

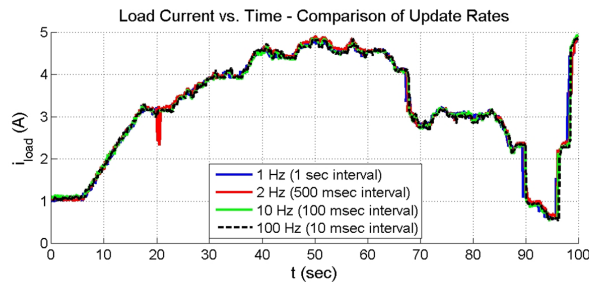


Fig. 7. Load current as a function of informatic control update rate.

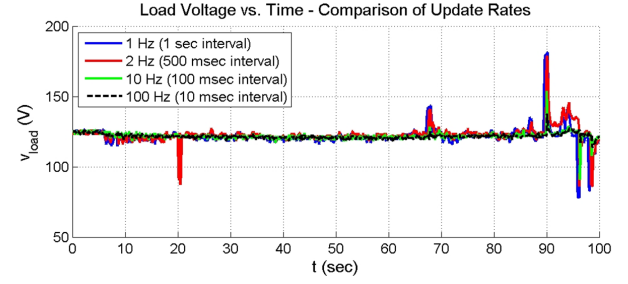


Fig. 8. Bus voltage as a function of informatic control update rate.

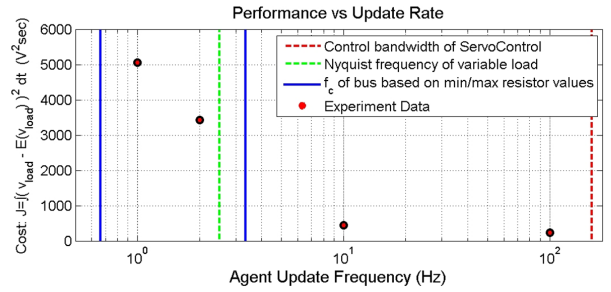


Fig. 9. Computed cost for each experiment without energy storage.

considered; these included: 1Hz, 2 Hz, 5 Hz, 10 Hz, 30 Hz, 50 Hz and 100 Hz. The energy storage (ARESE-A) output currents are shown in Fig. 10 for select update rates. To

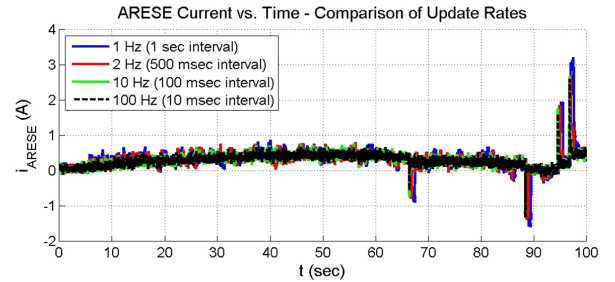


Fig. 10. Energy storage (ARESE-A) output current as a function of informatic control update rate.

consider system performance in terms of the energy storage control effort, the cost function was redefined as follows

$$J = \int_{t_0}^{t_f} (i_{ARESE}(\tau) - E(i_{ARESE}))^2 d\tau \quad (11)$$

The computed costs are plotted against update rate and shown in Fig. 11.

C. Two variable wind turbine variable load

The two sources in this experiment are both stochastic sources (i.e. wind turbine) based on the system defined

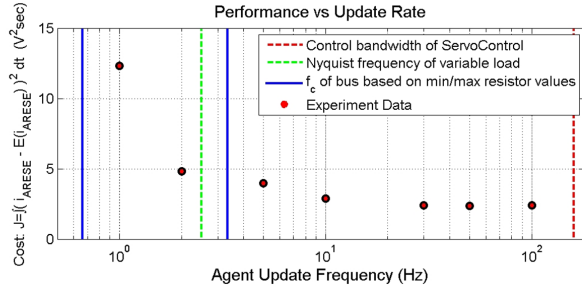


Fig. 11. Computed cost for each experiment with energy storage.

in [12] and the digital resistor is capable of 64 resistance values that may be scripted from the master control console. The two wind profiles used for this experiment are shown in Fig. 12 and the corresponding load profile is shown in Fig. 6, respectively.

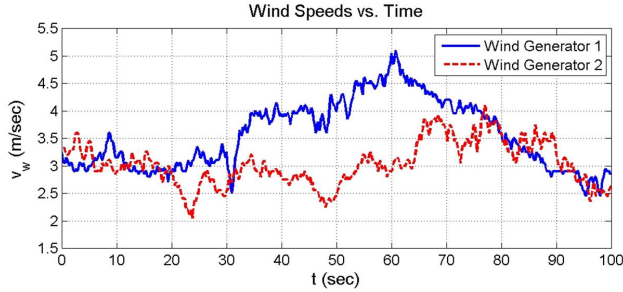


Fig. 12. Two wind turbines: wind profiles.

The corresponding microgrid responses are shown for currents in Fig. 13, bus voltage in Fig. 14, boost converter duty cycles in Fig. 15, and the energy storage response nearest to wind generator (ARESE-B) in Fig. 16.

VI. MULTIPLE MICROGRID SYSTEM NAVY ELECTRIC SHIP CONFIGURATION

Future Navy electric ship system designs will require advanced power and energy storage systems that will need improved control, design and analysis techniques. Initially, the baseline design that is being investigated consists of star-board (microgrid 1), port (microgrid 2), and a load (microgrid 3) collective system. The multiple microgrid system with tertiary level control is shown schematically in Fig. 17.

The first step in evaluating different design scenarios will investigate distributed energy storage and multi-layer feedback and communication update rates. The next section lays out the dynamic optimization design that will be used in future studies to evaluate multiple configuration scenarios and proved optimal set-points with respect to varying cost functions.

A. Optimization for Multiple Microgrids

In order to formulate the optimal control problem, one can model the microgrid as a circuit comprised of five

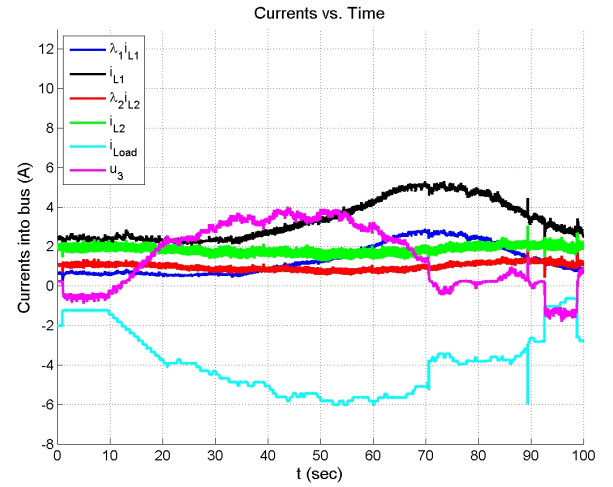


Fig. 13. Two wind turbines: currents.

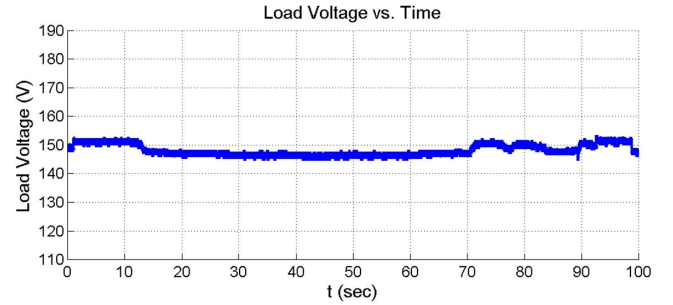


Fig. 14. Two wind turbines: bus voltage.

pieces: boost converters (component A), DC buses (component B), connections between a DC bus and a transmission line (component C), transmission lines (component D), and additional loads (component E) on the DC buses. These components A-E, are shown with their diagrams in Fig. 18. This modularization allows one to quickly formulate a new microgrid on an arbitrary topology. As for the optimization formulation itself, let Fig. 18 define the individual circuit components. In addition, one can define the following

p	$\in \mathcal{N}$	# of DC buses
q	$\in \mathcal{N}$	# of transmission lines
m	$\in \mathcal{N}^p$	# of boost converters connected DC bus
m_L	$\in \mathcal{N}^p$	# of additional loads connected DC bus
E	$\in \mathcal{R}^{p \times q}$	connectivity matrix between DC buses and transmission lines where
	$E_{jk} =$	1, Bus j connected to transmission line j
		0, Otherwise
n_{DC}	$\in \mathcal{N}^p$	# of connections from DC buses,
		$\sum_{k=1}^q E_{jk}$
n_{TL}	$\in \mathcal{N}^q$	# of connections from transmission lines,
		$n_{TL_k} = \sum_{j=1}^p E_{jk}$

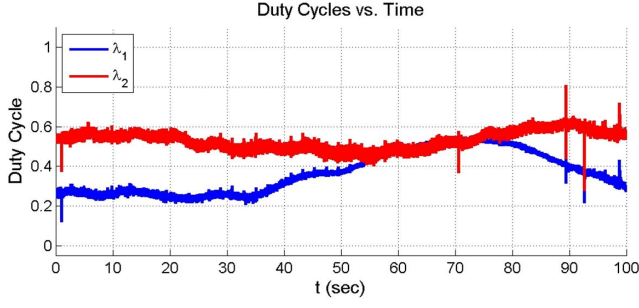


Fig. 15. Two wind turbines: lambda duty cycle controls.

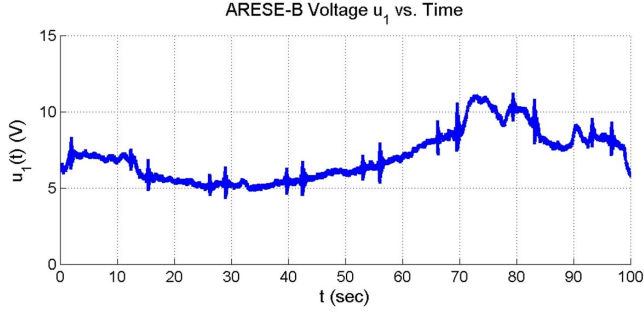


Fig. 16. Two wind turbines: energy storage at wind source.

$\kappa \in \Pi_{j=1}^p [\{1, \dots, n_{DCj}\} \rightarrow \mathcal{N}] = \text{indexing function that maps the connection from DC bus to the appropriate transmission line defined as}$

$$\kappa_j(l) = \arg \min \left\{ i \in \mathcal{N} : \sum_{k=1}^i E_{jk} \leq l \right\}.$$

$\iota \in \Pi_{k=1}^q [\{1, \dots, n_{TLk}\} \rightarrow \mathcal{N}] = \text{indexing function that maps the connections from transmission line to the appropriate DC bus defined as}$

$$\iota_k(l) = \arg \min \left\{ i \in \mathcal{N} : \sum_{j=1}^i E_{jk} \leq l \right\}.$$

$\bar{s} \in \Pi_{j=1}^p [\mathcal{R} \rightarrow \mathcal{R}]^{n_{DCj}} = \text{two position switch in the connection between the DC buses } j \text{ and transmission lines defined as}$

$$\bar{s}_{jk}(\lambda) = \begin{cases} -1 & \text{switch position 1,} \\ \lambda & \text{switch position 2.} \end{cases}$$

$s \in \Pi_{j=1}^p [\mathcal{N} \rightarrow \mathcal{N}]^{n_{DCj}} = \text{two position switch in the connection between the DC buses and the transmission lines defined as}$

$$s_{jk}(\lambda) = \begin{cases} \lambda & \text{switch position 1,} \\ -1 & \text{switch position 2.} \end{cases}$$

This allows the optimal control problem to be formulated as minimize $u, \lambda, \dot{i}, \dot{v}_B, \dot{v}_B, u_B, u_C, \lambda_C, \dot{i}_C, \dot{i}_C, v_T, \dot{v}_T, u_T$ for the following performance index

$$PI_{multiple} = \frac{w_1}{2} (\|\lambda - \lambda_0\|^2 + \|\lambda_C - \lambda_{C0}\|^2)$$

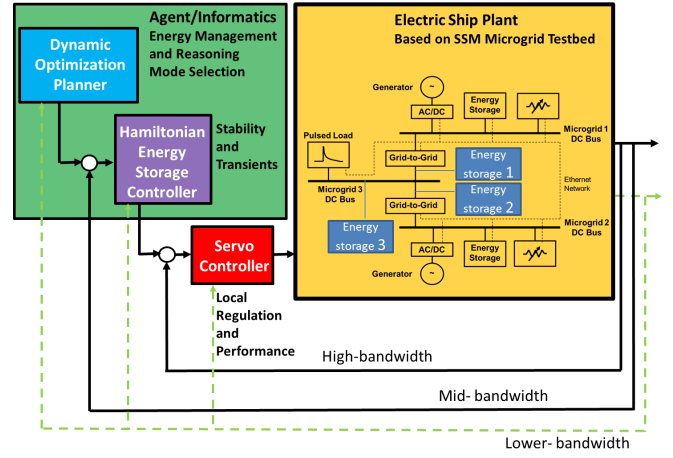


Fig. 17. Tertiary level control design for information flow and energy storage integration.

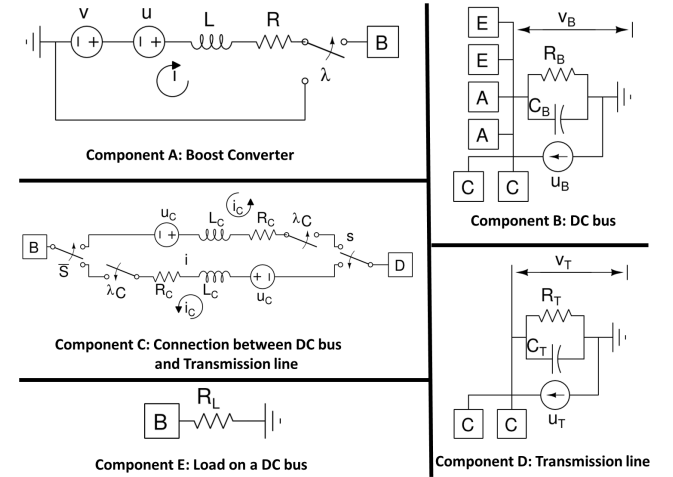


Fig. 18. Optizelle multiple microgrid components.

$$\begin{aligned} & + \frac{w_2}{2} (\|u\|^2 + \|u_B\|^2 + \|u_C\|^2 + \|u_T\|^2) \\ & + \frac{w_3}{2} (i^T \text{Diag}(R) i + i_C^T \text{Diag}(R_C) i_C) \\ & + \frac{w_4}{2} ((i^T u)^2 + (v_B^T u_B)^2 + (i_C^T u_C)^2 + (v_T^T u_T)^2) \quad (12) \end{aligned}$$

subject to: circuit equations, discretization equations, and the parameter bounds (see the Appendix for details).

In this formulation, one can minimize either the change in the boost convert duty cycle, the amount of storage used by the microgrid, the parasitic losses, or the amount of power. Constraints are then applied to the formulation by the circuit equations for the microgrid, a discretization in time, and by bounds on each individual parameters.

In order to solve the optimization formulation, the optimization solver called Optizelle[15] was employed which uses an inexact composite step SQP trust-region algorithm combined with a primal-dual interior point method. This allows one to solve the optimal control problem in roughly 10-20 iterations.

B. Simple multiple microgrid example

As an example, consider the microgrid in Fig. 19. Here,

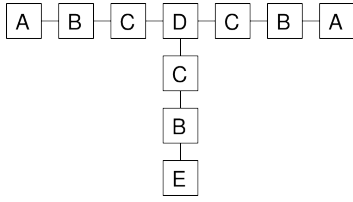


Fig. 19. Optizelle multiple microgrid configuration.

microgrids are on both the left and right that provide generation. These are connected to a transmission line, which connects to a third microgrid in the center that provides exclusively load (similar to the Navy electric ship setup). Using Optizelle, one can minimize the change in the boost converter duty cycles in 11 iterations as shown in Fig. 20.

Iter	f(x)	grad	dx	g(x)	mu_est
1	2.76e-02	1.38e-03	---	1.19e+03	1.00e+00
2	9.58e-02	1.62e-03	1.00e+03	2.74e+02	3.22e-01
3	2.43e-02	4.90e-03	2.00e+03	1.31e+00	8.51e-02
...					
9	6.44e-14	2.46e-08	5.13e+02	7.00e-05	8.92e-07
10	7.30e-14	1.01e-10	3.81e+02	8.42e-05	8.91e-08
11	1.59e-11	3.79e-08	3.95e+02	8.28e-05	8.91e-09

Fig. 20. Optizelle numerical convergence multiple microgrid results.

VII. SUMMARY AND CONCLUSIONS

In this paper a method for designing feedback controllers for integration of stochastic sources and loads into DC microgrid and multiple microgrid systems was presented. The system under test was described, and a discussion of SSM hardware capabilities and performance reviewed. A dynamic optimization planner, based on the Optizelle toolset, was developed for the guidance controls block. A HSSPFC controller design, incorporating energy storage systems provided static and dynamic stability conditions. Experimental results showed critical trade-off between the informatics/communication update rates versus the energy storage system requirements. A second experiment for stochastic sources and loads demonstrated stable voltage regulation and provided energy storage specifications from the SSM testbed ARESE (A/B) emulators. The extension to multiple microgrids and its application to electric Navy ship microgrids was introduced which utilizes Optizelle's flexible component building blocks for general microgrid configurations. Future work will highlight new configurations, HSSPFC designs and detailed performance testing specific to Navy ship scenarios.

ACKNOWLEDGMENTS

Sandia National Laboratories is a multiprogram laboratory operated by Sandia Corporation, a Lockheed Martin Company, for the U.S. Department of Energy's National Nuclear Security Administration under contract DE-AC04-94AL85000. The authors would like to acknowledge Professor Gordon Parker and Research Professor Steven Goldsmith at Michigan Technological University for their early support in optimization cost function formulations and informatics/agent based architectures, respectively. A large portion of this research was sponsored by a GC/LDRD microgrid. [16]. The authors also acknowledge our NAVSEA Naval Power Systems, Electric Ship PMS 320 program for their support.

REFERENCES

- [1] Robinett R.D. III and Wilson, D.G., **Nonlinear Power Flow Control Design: Utilizing Exergy, Entropy, Static and Dynamic Stability, and Lyapunov Analysis**, Springer-Verlag, London Ltd., Oct. 2011.
- [2] Dohn, R.L., *The business case for microgrids: the new face of energy modernization*, 2011, Siemens AG White paper.
- [3] Farhangi, H., *The Path of the Smart Grid*, IEEE Power Energy Mag., Vol. 8, No. 1, pp. 18–28, Jan./Feb. 2010.
- [4] Guerrero, J.M., Vasquez, J.M., Garcia de Vicuna, L., Castilla, M., *Hierarchical Control of Droop-Controlled AC and DC Microgrids - A General Approach Toward Standardization*, IEEE Transactions on Industrial Electronics, Vol. 58, No. 1, January 2011, pp. 158–172.
- [5] Hiayi, H., Chuanwen, J., and Rong, X., *A Review on Distributed Energy Resources and MicroGrid*, Renew. Sustain. Energy Rev., Vol. 12, No. 9, pp. 2472–2483, Dec. 2008.
- [6] Tulpule, P., Yurkovich, S., Wang, J., and Rizzoni, G., *Hybrid Large Scale System for a DC Microgrid*, American Control Conference (ACC), 2011, pp. 3899–3904, San Francisco, CA.
- [7] Wilson, D.G., Robinett III, R.D., and Goldsmith, S.Y., *Renewable Energy Microgrid Control with Energy Storage Integration*, International Symposium on Power Electronics, Electrical Drives, Automation and Motion (SPEEDAM), June 20–22, 2012, Sorrento, Italy.
- [8] Robinett, R.D. III, Wilson, D.G., Eisler, G.R., Hurtado, J.E., **Applied Dynamic Programming for Optimization of Dynamical Systems**, SIAM, Advances in Design and Control Series, July 2005.
- [9] Robinett, R.D. III, and Wilson, D.G. *Nonlinear Power Flow Control Design for Combined Conventional and Variable Generation Systems: Part I - Theory*, 2011 IEEE Multi-Conference on Systems and Control, Sept. 26–30, 2011, Denver, Co., USA, pp. 61–64.
- [10] Robinett, R.D. III, and Wilson, D.G. *Transient Stability and Performance Based on Nonlinear Power Flow Control Design of Renewable Energy Systems*, 2011 IEEE Multi-Conference on Systems and Control, Sept. 26–30, 2011, Denver, Co., USA, pp. 881–886.
- [11] Neely, J., Pekarek, S., Glover, S., Finn, J., Wasynczuk, O., and Loop, B., *An Economical Diesel Engine Emulator for Micro-grid Research*, International Symposium on Power Electronics, Electrical Drives, Automation and Motion (SPEEDAM), June 20–22, 2012, Sorrento, Italy.
- [12] Neely, J., Glover, S., Wasynczuk, O., and Loop, B., *Wind Turbine Emulation for Intelligent Microgrid Development*, IEEE Cyber 2012 Conference, May 27–31, 2012, Bangkok, Thailand.
- [13] Glover, S., Neely, J., Lentine, A., Finn, J., White, F., Foster, P., Wasynczuk, O., Pekarek, S., and Loop, B., *Secure Scalable Microgrid Test Bed at Sandia National Laboratories*, IEEE Cyber 2012 Conference, May 27–31, 2012, Bangkok, Thailand.
- [14] Neely, J.C., Ruehl, K.M., Jepsen, R.A., Roberts, J.D., Glover, S.F., White, F.E., and Horry, M.L., *Electromechanical Emulation of Hydrokinetic Generators for Renewable Energy Research*, OCEANS'13 MTS/IEEE Sand Diego, September 2013.
- [15] Young, J., *Optizelle: An open source software library designed to solve general purpose nonlinear optimization problems*, 2014, www.optimojoe.com, Open source software.
- [16] Glover, S.F., et. al., *Enabling Secure Scalable Microgrids for High Penetration Renewables: Final Report for LDRD Project #152503*, Sandia National Laboratories, Sand Report SAND2013-10704, December 2013.

APPENDIX

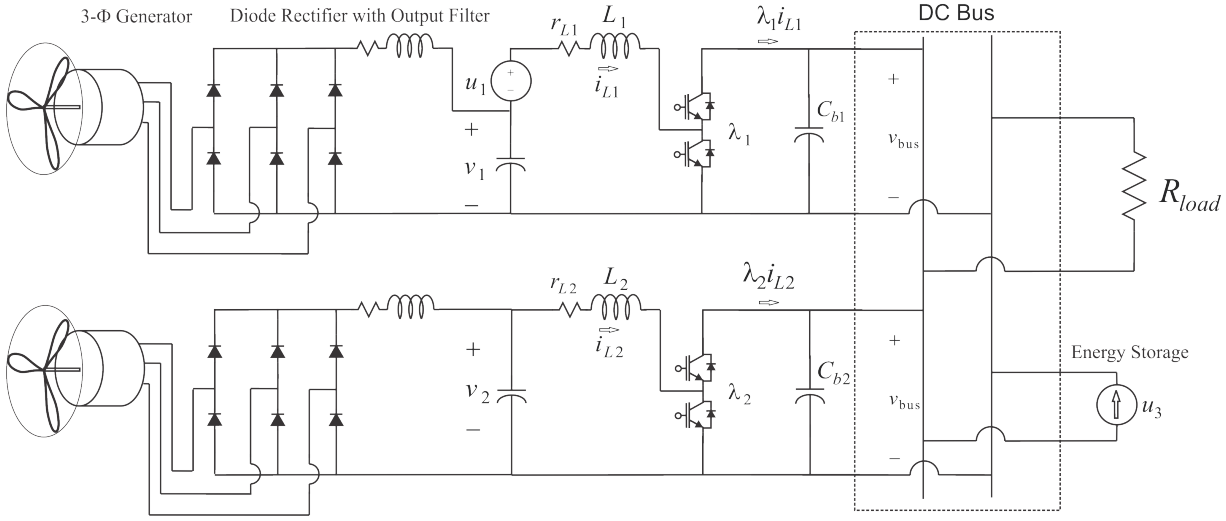


Fig. 21. Schematic of a single DC microgrid, as one part of a three microgrid collective.

Circuit equations

$$L_{ij} \dot{i}_{ij} = -R_{ij} i_{ij} - \lambda_{ij} v_{Bj} + v_{ij} + u_{ij}$$

$$C_{Bj} \dot{v}_{Bj} = \left(\sum_{i=1}^{m_j} \lambda_{ij} i_{ij} \right) - \frac{1}{R_{Bj}} v_{Bj} - \left(\sum_{i=1}^{m_{Lj}} \frac{1}{R_{Li}} \right) v_{Bj} + u_{Bj} + \left(\sum_{l=1}^{n_{DCj}} \bar{s}_{j\kappa_j(l)} (\lambda_{Cj\kappa_j(l)}) i_{Cj\kappa_j(l)} \right)$$

$$L_{Cj\kappa_j(l)} \dot{i}_{Cj\kappa_j(l)} = -R_{Cj\kappa_j(l)} i_{Cj\kappa_j(l)} - s_{j\kappa_j(l)} (\lambda_{Cj\kappa_j(l)}) v_{T\kappa_j(l)} - \bar{s}_{j\kappa_j(l)} (\lambda_{Cj\kappa_j(l)}) v_{Bj} + u_{Cj\kappa_j(l)}$$

$$C_{Tk} \dot{v}_{Tk} = \left(\sum_{l=1}^{n_{TLk}} s_{\iota_k(l)k} (\lambda_{C\iota_k(l)k}) i_{C\iota_k(l)k} \right) - \frac{1}{R_{Tk}} v_{Tk} + u_{Tk}$$

$$1 \leq j \leq p, \quad 1 \leq i \leq m_j, \quad 1 \leq k \leq q, \quad 1 \leq l \leq n_{DCj}$$

Discretization equations

$$i = i_0 + \Delta t \dot{i}$$

$$v_B = v_{B0} + \Delta t \dot{v}_B$$

$$i_C = i_{C0} + \Delta t \dot{i}_C$$

$$v_T = v_{T0} + \Delta t \dot{v}_T$$

Parameter bounds

$$i_{\min} \leq i \leq i_{\max}$$

$$i_{C\min} \leq i_C \leq i_{C\max}$$

$$u_{\min} \leq u \leq u_{\max}$$

$$u_{B\min} \leq u_B \leq u_{B\max}$$

$$u_{C\min} \leq u_C \leq u_{C\max}$$

$$u_{T\min} \leq u_T \leq u_{T\max}$$

$$\lambda_{\min} \leq \lambda \leq \lambda_{\max}$$

$$\lambda_{C\min} \leq \lambda_C \leq \lambda_{C\max}$$